Mueller matrix spectroscopic ellipsometry of a thin ZnO anisotropic crystal layer and its optical properties

Author: Michelle Fernanda Cruz Palma.

*Facultat de Física, Universitat de Barcelona, Diagonal 645, 08028 Barcelona, Spain.**

Advisor: Jordi Gomis Brescó.

***Abstract**: We have determined the optical properties (ordinary and extraordinary index of refraction) of a thin anisotropic uniaxial sample of ZnO on a glass substrate, using a 4-photoelastic modulator polarimeter (4PEM). The analysis was done by shining a light beam on two points of the sample, to analyse its inhomogeneity, and by 3 different incidence angles for each point. Using a preesxisting Matlab code to fit the 4PEM results, the coefficients of the Mueller Matrix (MM) were simulated for each wavelength, from 400 nm to 800 nm, and then the indices of refraction were calculated using a Sellmeier expression and compared with the values of ZnO bulk monocrystal from the bibliography.*

I. INTRODUCTION

The Mueller matrix (MM) developed in 1943 by Hans Mueller, describes how light is altered by an optical element based on experimentally observable quantities. Stokes vectors (S) describe the properties of light with different light intensity measurements for different polarization states. MM links the input and output Stokes vector following the interaction of electromagnetic radiation with an optical medium by reflection, transmission, or scattering, as follows [1]:

$$\boldsymbol{S_{out} = MS_{in}} \tag{1}$$

S is a real-valued $\mathbf{4 \times 1}$ vector defined by:

$$\boldsymbol{S} = \begin{bmatrix} S_0 \\ S_1 \\ S_2 \\ S_3 \end{bmatrix} = \begin{bmatrix} I_x + I_y \\ I_x - I_y \\ I_{+45^\circ} - I_{-45^\circ} \\ I_R - I_L \end{bmatrix} \tag{2}$$

where $\boldsymbol{I_x, I_y, I_{\pm 45}}^\circ$ corresponds to the intensities of linear polarized light oriented along the respective subscript direction and $\boldsymbol{I_R, I_L}$ to right and left circular polarizations, respectively.

Both normalized arrays, $m_{ij} = \boldsymbol{M_{ij}/M_{00}}$ and $\boldsymbol{S/S_0}$, are generally used such that the coefficients are limited to values between ±1.

$\boldsymbol{M}$ is a real-valued $\mathbf{4 \times 4}$ matrix where $\boldsymbol{M_{00}}$ corresponds to the unpolarized input light beam attenuation; $\boldsymbol{m_{01}, m_{02}, m_{03}}$ represent the diattenuation; $\boldsymbol{m_{10}, m_{20}, m_{30}}$ describe the polarizance; and the rest are associated with retardance (the lowercase letters denote the normalized coefficients by $\boldsymbol{M_{00}}$).

From a simulation point of view, it is possible to determine how light is reflected, transmitted and absorbed by the material using its optical properties, described by the complex refractive index ($\boldsymbol{\tilde{n}}$) or the dielectric function ($\boldsymbol{\tilde{\varepsilon}}$), which are defined as follows [1]:

$$\boldsymbol{\tilde{\varepsilon} = \varepsilon_1 - i\varepsilon_2 = \tilde{n}^2 = (n - ik)^2} \tag{3}$$

where $\boldsymbol{n}$ is the index of refraction, which describes the phase velocity of light, and $\boldsymbol{k}$ is the extinction coefficient, which describes light absorption.

Given that ZnO, the focus of this study, is a wide-band semiconductor that can be grown as a hexagonal wurtzite-like uniaxial crystal [2], it exhibits two distinctly defined optical properties: the ordinary and extraordinary indices of refraction, which are always perpendicular and parallel to the optic axis, respectively. The real part of these indices will be assumed to follow Sellmeier formulas [3], respectively:

$$n_o = \sqrt{1 + A_o \cdot \frac{\lambda^2}{(\lambda^2 - \lambda_{0o}^2)}} \tag{4}$$

$$n_e = \sqrt{1 + A_e \cdot \frac{\lambda^2}{(\lambda^2 - \lambda_{0e}^2)}} \tag{5}$$

where $A_o, A_e, \lambda_{0o}, \lambda_{0e}$ are fit parameters representing the ordinary and extraordinary amplitudes and resonant wavelengths, respectively. These parameters are determined based on the MM coefficients obtained within a specified wavelength range. Materials exhibiting directional-dependent indices are termed birefringent. They are characterized by their birefringence ($\Delta n = n_e - n_o$) which, for instance, leads to the phenomenon of double refraction, where the incident beam splits into two linearly polarized beams perpendicular to each other under oblique incidence. Since the index of refraction is linked to the phase velocity of light, the birefringence, along with the path-length, determines the retardance between orthogonal light waves traveling through the material along the ordinary and extraordinary axes [1].

* Electronic address: tfgac@ub.edu

Spectroscopic ellipsometry [1] is a technique used to measure the polarization change resulting from the interaction of polarized light with a sample, whether through reflection or transmission. In ellipsometry measurements, it's common to distinguish between electric fields vibrating parallel to the plane of incidence (p-polarized) and those perpendicular to the plane of incidence (s-polarized), as illustrated in Fig.(1). The MM structure for the sample used in our study, which is uniaxial with the optical axis perpendicular to its surface, is the same as the MM for isotropic samples at oblique angles of incidence. Thus, the MM is symmetric with $m_{00} = m_{11} = 1, m_{10} = m_{01}, m_{22} = m_{33}, m_{32} = -m_{23}$ and the remaining terms are equal to 0. In the case of isotropic samples, the optical properties remain consistent across all directions. However, at different orientations the transmission varies, leading to distinct experimental results for each incidence angles, whether the sample is isotropic or anisotropic. The determination of material anisotropy relies on the goodness of fit when compared to an anisotropic model, unlike the fit with an isotropic model where $n_o = n_e$. Therefore, it's crucial to take measurements at various angles since at a singular angle we cannot differentiate between isotropic and anisotropic properties, as the results could seemingly align with both models.

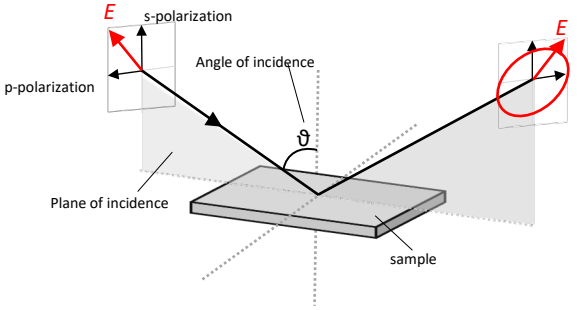

FIG. 1: Ellipsometry measurement at an oblique angle, θ, where the plane of incidence encompasses the incident light, the reflected light, and the normal to the sample surface. When the incident light is linearly polarized, the reflected light can, in general, become elliptically polarized. The p-polarized and s-polarized electric fields refer to vibration parallel and perpendicular to the plane of incidence, respectively.

II. DEVELOPING SECTIONS

A. EXPERIMENTAL METHOD

In this analysis, a spectroscopic Mueller matrix polarimeter with four photoelastic modulators (PEMs) and no moving parts is used, as depicted Fig.(2). All the MM elements are simultaneously determined by analysing the frequencies of the time-dependent intensity of the light beam. This is because the detected information is a modulated signal, wherein relative polarization changes are detected rather than absolute intensities [4]. The use of 4PEMs offers the advantage of high-sensitivity measurement of polarization properties. In previous projects, thin layers of ZnO have also been analysed, but it is likely that these studies either assumed the material to be isotropic or grew polycrystals orientated randomly, exhibiting isotropic behaviour, resulting in a single isotropic index of refraction. Hence, the importance of this project lies in the capability of our device, under suitable growing conditions, to accurately measure both the ordinary and extraordinary refraction indices even for very thin layers with great precision, considering the anisotropies of the sample.

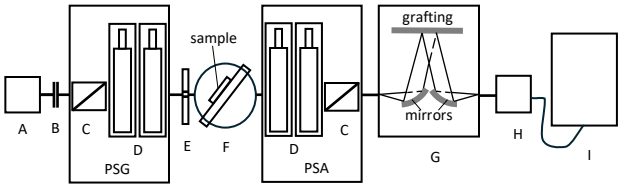

FIG. 2: Schematic diagram of the 4-PEM. Light travels from left to right. A: Xenon arc lamp. B: Collimator lenses. PSG that contains C: Polarizer and D: Photoacoustic modulators. E: Iris. F: Rotation stage. PSA that contains: D: Photoacoustic modulators and C: Polarizer. G: Spectrometer. H: PMT – Photomultiplier. I: Computer.

The operation involves a xenon light source (A) emitting light, which is then directed through collimator lenses (B) and directed towards the Polarization State Generator (PSG). The PSG comprises a polarizer (C) and two photoacoustic modulators (D). Subsequently, the light passes through an iris (E) and reaches the rotation stage (F), where it interacts with the sample under investigation. After the sample interaction, the Polarization State Analyzer (PSA), consisting of identical elements as the PSG but positioned oppositely, determines the altered polarization state of the light. The light beam is then directed towards the spectrometer (G), passing through a collimating mirror, a reflection grafting, and a focusing mirror, before reaching the detector (H). The intensity of light is measured depending on the wavelength and analysed using a computer data processing system (I). To minimize contamination from ambient light sources, the detector is covered with black fabric, room lights are dimmed, and blinds are drawn.

Before starting to take the measurements, calibration of 4PEM is essential to ensure accurate and precise measurement of light polarization. Calibration procedures include system alignment, modulator phase, amplitude calibration, phase effects compensation and linearity verification. Since the experimental setup was already assembled, our task was to confirm that, in transmission and without sample, the MM obtained was the identity matrix, corresponding to that of air. To be able to measure the desired oblique angle, it was necessary to adjust the normal incidence angle of light on the rotation stage ($\theta_{ref} = 0$), serving as a reference point.

The concepts of coherence and incoherence of light must be considered. If spatial coherence is met, which pertains to the extent to which a beam of light can maintain phase synchronization over distance, two forward propagating beams interfere, if not, beam intensities add incoherently. This condition is met only if a critical distance in our system, for instance the thickness of any layer, doesn't surpass a certain value known as the coherence length [5].

The utilization of a thick uniaxial material, as employed by Jellison [3], produces incoherent addition of light intensities due to the thickness surpassing the coherence length. When measuring thin layers deposited on thick substrates, both coherence interference and incoherent intensity addition effects are present. In our case, an anisotropic thin layer of ZnO, approximately the order of the wavelength of light, (preserving coherence of the incident and reflected beams) is deposited on an isotropic glass substrate with a thickness significantly greater than the wavelength of light. Withing the thick glass substrate, coherence is entirely lost, resulting in no oscillations in the transmission measurements. Conversely, in the thin ZnO layer, coherent overlap and interference of light reflections occur, resulting in oscillations in transmission. Indeed, the presence of an interference oscillation allows to determine the layer thickness with great accuracy.

B. MEASUREMENTS AND RESULTS

The measurements were made in a wavelength range between 400 nm and 800 nm, encompassing six different conditions of light incidence through the sample. These conditions involved measuring at two points—one at the top and the other in the middle of the sample, as illustrated in Fig. (3)—for each of three different oblique angles: 45º, 55º, and 65º.

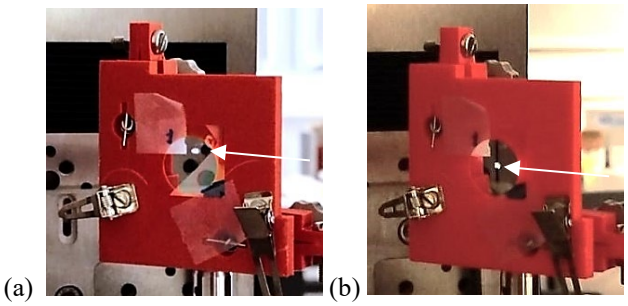

(a) (b)

FIG. 3: Experimental assembly in the laboratory where the points of impact of the beam on the sample are indicated. a) On top of the sample. b) In the middle of the sample.

The resulting MM coefficients for each condition are shown in Fig. (4):

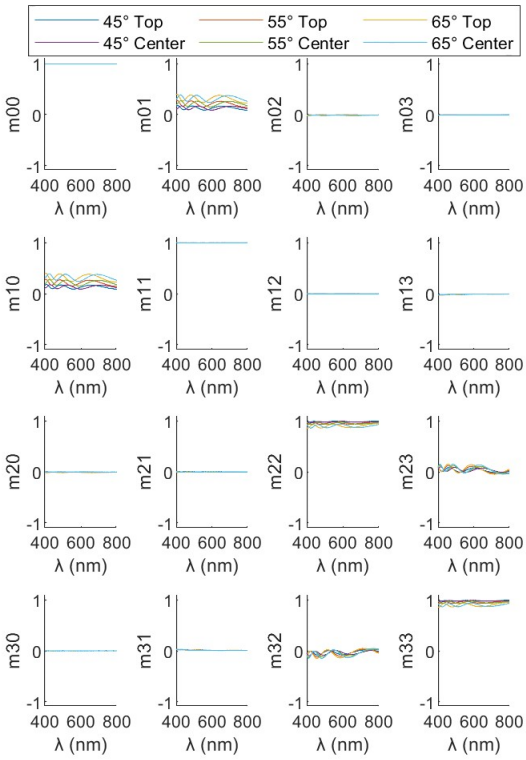

FIG. 4: Normalized Mueller matrix coefficients for 45º, 55º and 65º oblique angles of incidence at top and middle points of ZnO sample, over the entire measured wavelength range (400 nm – 800 nm).

As we can see the MM is symmetric such that $\boldsymbol{m_{00} = m_{11} = 1}$, $\boldsymbol{m_{10} = m_{01}}$, $\boldsymbol{m_{22} = m_{33}}$, $\boldsymbol{m_{32} = -m_{23}}$, which vary depending on the incidence angle, and the rest of terms are equal to 0 for each angle. Henceforth, we will show only $\boldsymbol{m_{01}}$, $\boldsymbol{m_{22}}$ *and* $\boldsymbol{m_{23}}$ elements, as illustrated in Fig.(6). Furthermore, the coefficients exhibit oscillations as a function of wavelength, indicative of coherent overlap and interference within the thin layer. Additionally, it is noted that the angle of incidence varies slightly the area of incidence of the light beam on the sample, that becomes greater as the oblique angle increases, although the central point of incidence remains fixed, as depicted in Fig.(5). Due to the strong inhomogeneity of our sample, that area change affects our measurements.

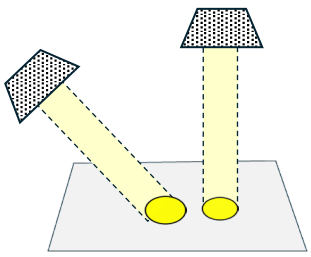

FIG. 5: Schema illustrating the dependence of the area of light coverage on the oblique angle of incidence, for the same light source.

Next, we adapt the Matlab code developed by Nichols et al [6] to compare simulations with our experiment results and fit them, as shown in Fig.(4), At this point, it's necessary to set up suitable $\boldsymbol{A_o}$, $\boldsymbol{\lambda_{0o}}$, $\boldsymbol{A_e}$, $\boldsymbol{\lambda_{0e}}$ and $\boldsymbol{d}$ parameters considerably close to the values that fit our data. To achieve this, we adopt the values found by Jellison [3] as initial guess and test different possible thicknesses ($\boldsymbol{d}$). From these values, the code determines the most accurate parameters corresponding to our experimental data, as shown in Table I.

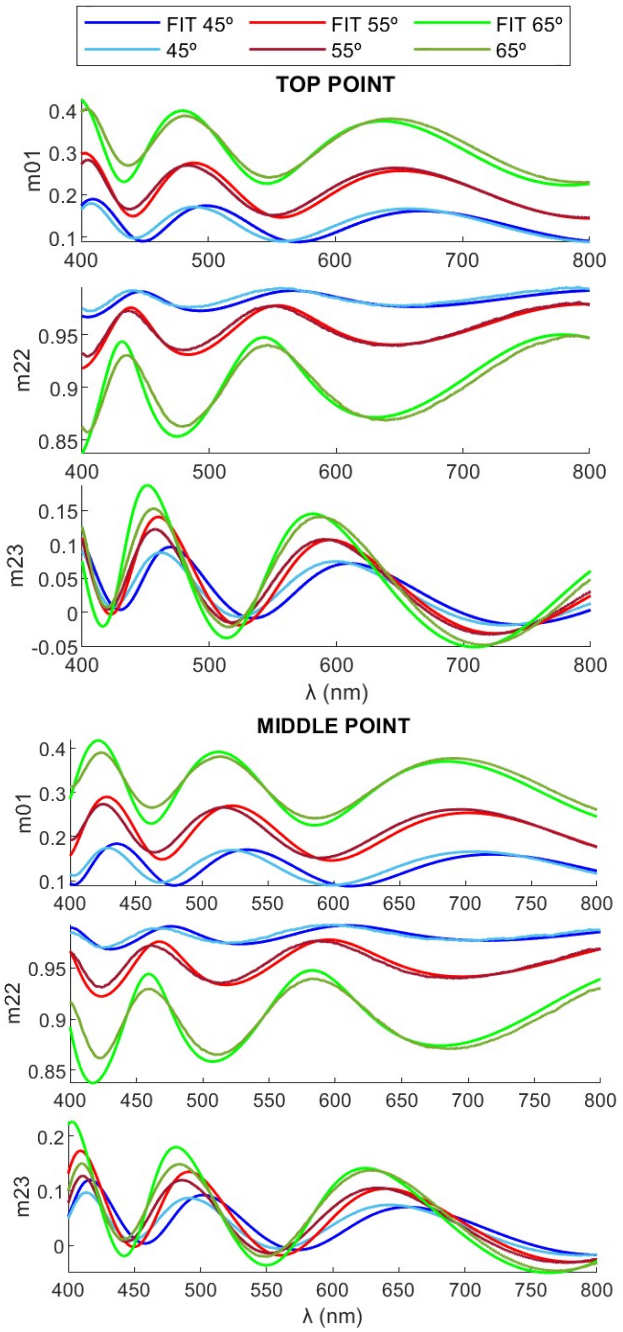

FIG. 6: Mueller matrix coefficients $\boldsymbol{m_{01}, m_{22}, m_{23}}$ for top and middle points of our sample, corresponding to our data and to the fitting function, for each oblique angle.

TABLE I: Sample thickness, ordinary amplitude, ordinary resonant wavelength, extraordinary amplitude and extraordinary resonant wavelength for top and middle points of our sample and for Jellison data [3], with their respective errors.

POINT	TOP	MIDDLE	JELLISON
$\boldsymbol{d}$ $(\boldsymbol{nm})$	475.4 ± 0.5	516.0 ± 0.5	*bulk*
$\boldsymbol{A_o}$	2.331 ± 0.005	2.322 ± 0.005	2.658 ± 0.002
$\boldsymbol{\lambda_{0o}(nm)}$	220.6 ± 0.5	216.6 ± 0.6	206.0 ± 0.4
$\boldsymbol{A_e}$	2.435 ± 0.006	2.464 ± 0.007	2.718 ± 0.002
$\boldsymbol{\lambda_{0e}(nm)}$	232.8 ± 0.7	219.6 ± 0.7	206.2 ± 0.4

Subsequently, from the parameters determined above and those given by Jellison, we use Sellmeier functions, as described in Eq. (4) and Eq. (5), to determine the ordinary and extraordinary indices of refraction of our sample as a function of wavelength. We then compare to the values corresponding to the Jellison monocrystal within the valid wavelength range [3] for each case. These results are plotted in Fig. (7).

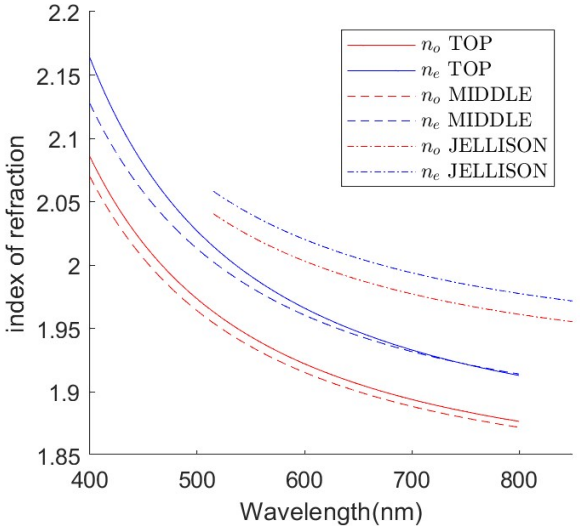

FIG. 7: Ordinary and extraordinary refractive index at top and middle points of our ZnO sample, over the entire measured wavelength range (400-800 nm), in comparison to the ZnO bulk of Jellison over his valid wavelength range (515-850 nm).

As we can see, although the values differ across the three cases, they remain comparable, so the results are accurate with very good precision. This variance arises due to the distinct characteristics of our and Jellison samples, despite they are the same material: ours is a thin layer while Jellison's is a large single crystal, and furthermore, the growth processes are very different. While Jellison's single crystal was commercially obtained with a determined thickness, we have grown monolayers via radio frequency (RF) magnetron sputtering. Under our growth conditions, the thin layers possessed enough energy to self-assemble forming ordered ZnO, so that the polycrystals have been

preferably oriented in a direction with the optical axis upward, enabling the observation of its anisotropic behaviour. It's well-known that modifying the growth conditions such as the substrate temperature, the argon residual gas pressure, the RF source power, etc., can directly affect both the quality of the material and the optical properties, as they are directly correlated. Consequently, by carefully controlling the growth parameters, we can optimize the material's characteristics to meet specific requirements for various applications.

III. CONCLUSIONS

The spectroscopic Mueller matrix polarimeter with four photoelastic modulators (4PEMs) we have in the laboratory, is currently the most precise instrument for determining the optical properties of a sample. In this study, it enabled us to accurately measure the thickness of a thin layer of ZnO at a specific point on the sample. Unlike previous studies, we successfully determined both the ordinary and extraordinary indices of refraction ($n_o \neq n_e$). The oscillations observed in the transmission measurements, along with the excellent fit to the model, underscore the importance of taking measurements at different incidence angles. These factors allowed us to identify the sample as an anisotropic material. Our analysis enables the characterization of a sample grown by RF magnetron sputtering on a glass substrate, where the polycrystals are oriented in a specific direction. In contrast, Jellison's study focused on a commercially available large crystal. When comparing these two samples, we observed that the optical properties of our ZnO layer are qualitatively similar, despite the significant differences in their intrinsic properties and growth processes. The significance of these results lies in the demonstration of a novel, cost-effective method for the growth of a thin ZnO layer, which exhibits anisotropic monocrystalline properties. This technique presents an alternative to exploit anisotropy in ZnO compared to the thick single crystals. Additionally, we have validated the accuracy of results obtained using the 4PEM polarimeter for characterizing extremely thin layers, which are challenging to measure with other instruments.

Acknowledgments

First, I want to thank Jordi Gomis Brescó who, as my advisor on this project, has helped me a lot and has always been at my disposal, making it very enjoyable. He has resolved my doubts and always guided me very well, both in the laboratory and when writing this report. I also want to thank my family, boyfriend and friends, who have always supported and encouraged me during this project.

[1] J. N. Hilfiker, N. Hong, and S. Schoeche, "Mueller matrix spectroscopic ellipsometry," *Advanced Optical Technologies*, vol. 11, issue 3-4, pp 59-9, June 2022.

[2] S. Nichols. "Coherence in polarimetry," Degree dissertation, Dept. Chem., NY Univ., U.S, 2018.

[3] G. E. Jellison, "Optical functions of uniaxial zinc oxide (ZnO) revisited," *Surface Science Spectra*, vol. 30, issue 2, pp 026001, Dec. 2023.

[4] O. Arteaga, et al., "Mueller matrix polarimetry with four photoelastic modulators: theory and calibration," *Applied optics,* vol. 51, issue 28, pp 6805-6817, Oct. 2012.

[5] C. P. Justiniano, "Interferencias", in *Optica*, Ed. 7, Zaragoza: Librería PONS, 1994, pp 239-276.

[6] S. Nichols, O. Arteaga, A. Martin, and B. Kahr, "Measurement of transmission and reflection from a thick anisotropic crystal modeled by a sum of incoherent partial waves," *Journal of the Society of America A,* vol. 32, issue 11, pp 2049-2057, Nov. 2015.